RSC Advances

PAPER

View Article Online
View Journal | View Issue

Cite this: *RSC Adv.*, 2015, **5**, 36307

Preparation of α-Fe_2O_3 films by electrodeposition and photodeposition of Co–Pi on them to enhance their photoelectrochemical properties

Jin You Zheng, Se In Son, Thanh Khue Van and Young Soo Kang*

Received 17th February 2015
Accepted 13th April 2015

DOI: 10.1039/c5ra03029c

www.rsc.org/advances

In this paper, α-Fe_2O_3 photoanodes with different structures were prepared on indium-doped tin oxide (ITO) coated glass by calcination of electrodeposited α-Fe films. Morphologies of the films can be varied from the nanoparticle to sparse dendrites, and then to high-density dendrites as the deposition time is prolonged. Their morphology-dependent photoelectrochemical properties with and without coupling with the photodeposited Co–Pi were investigated through the photocurrent and the photoresponse. The α-Fe_2O_3 film exposing a larger area of the bottom layer has a low photocurrent onset potential; after coupling with the Co–Pi co-catalyst, their onset potentials are shifted to the negative direction. The photocurrent of hematite films can be enhanced more than 40% for the particle type and 70% for the dendritic type regardless of low photocurrent values. This indicates that the photodeposited Co–Pi can effectively suppress the photogenerated electron–hole recombination on the surface of hematite, especially dendritic α-Fe_2O_3.

1. Introduction

In 1972, Fujishima and Honda first reported the photoelectrochemical (PEC) production of H_2 and O_2, *via* a water splitting reaction with photo-generated electrons and holes (e^-–h^+), at chemically biased TiO_2 under UV light illumination.[1] This report attracted great attention not only of electrochemists but also of many scientists in a broad area, and numerous related studies were reported from the 1970s to now.[2] Nowadays, many other semiconductor materials such as α-Fe_2O_3, WO_3 and $BiVO_4$ are widely investigated for PEC water splitting with external bias or direct solar water splitting. Among them, α-Fe_2O_3 (hematite) is one of the most popular n-type semiconductors for use as a photoanode in the water splitting PEC cell. It is very abundant on earth, low in cost, environmentally benign and capable of withstanding neutral and alkaline condition.[3,4] Above all, for solar water splitting, it has a narrow indirect band gap of ~2.1 eV that could utilize about 40% of the incident solar spectra,[5] which is better than TiO_2 ($E_g \sim 3.0$ eV) and WO_3 ($E_g \sim 2.7$ eV). α-Fe_2O_3 possesses 15.3% of theoretical solar-to-hydrogen efficiency or 12.6 mA cm^{-2} of photocurrent at 1.23 *vs.* RHE under 1 sun irradiation.[6] Its valence band position has a sufficient overpotential for oxygen evolution reaction (OER).[4] However, α-Fe_2O_3 has several inherent drawbacks such as the very short hole-diffusion length (~2–4 nm), low electron mobility (~10^{-1} cm^2 V^{-1} s^{-1}) and high recombination rate of photo-generated e^-–h^+, poor electrical conductivity and low visible light absorption coefficient.[4,7,8] Many different strategies, such as nanostructuring, elemental doping and surface treatment, have been investigated to overcome these inherent drawbacks to achieve a high plateau photocurrent and/or low onset potential in hematite-based PEC devices.[9]

In 2008, Nocera *et al.*[10] reported a new type of oxygen-evolution catalyst with amorphous features composed of cobalt, oxygen, and phosphate elements, normally named as cobalt–phosphate (Co–Pi), which is formed *in situ* upon anodic polarization of an inert indium-tin-oxide coated glass (ITO) electrode in aqueous phosphate buffer solution at pH 7.0 containing Co^{2+} ions. The Co–Pi film can oxidize water at pH 7 with a current density of 1.0 mA cm^{-2} under a very low overpotential of 0.41 V. It can be possible structural and functional analogues to the Mn_3CaO_4–Mn cubane of the oxygen-evolving complex in photosystem II (PSII), where Co replaces Mn and the cubane is extended in a corner-sharing head-to-tail dimer.[10–15] This Co–Pi catalyst has been received much attention due to its ability to self-assemble under neutral conditions, its self-repair mechanism, and its formation from low-cost and earth-abundant elements.[10,16,17] Interestingly, when the Co–Pi was coupled with semiconductors, it considerably enhances the efficiency of solar water splitting.[14] Many works related with Co–Pi as a co-catalyst have been reported. For examples, Co–Pi can enhance the efficiency of water photooxidation when it was coupled with WO_3,[4] ZnO,[18] $BiVO_4$,[19–22] Si[23] and α-Fe_2O_3.[4,9,24–26] In presence of Co–Pi electrocatalyst on photoanodes as co-catalyst can not only enhance the photocurrent density, but also achieve negative shift of onset potential.[27] For examples, Wang *et al.*[21] reported

Korea Center for Artificial Photosynthesis (KCAP), Department of Chemistry, Sogang University, Seoul 121-742, Republic of Korea. E-mail: yskang@sogang.ac.kr; Tel: +82-2-705-8882

that the photocatalytic activity of O_2 evolution on Co–Pi/$BiVO_4$ can be greatly enhanced with 6.8 times comparison with that of bare $BiVO_4$ when the loading amount of Co–Pi is about 1.0 wt%. The photocurrent of $BiVO_4$ electrode also can be enhanced accompanied by the onset potential negatively shifted with optimal amount of Co–Pi loading. Recently, Kim *et al.*[6] have reported that a kind of wormlike hematite photoanode gives a photocurrent of 1.26 mA cm^{-2} at 1.23 V *vs.* RHE under 1 sun (100 mV cm^{-2}) and AM 1.5 G simulated solar light irradiation. After Pt doping (Pt:Fe_2O_3), the photocurrent increases by 74% to 2.19 mA cm^{-2}. When the Pt:Fe_2O_3 is modified again with Co–Pi co-catalyst, the photocurrent surprisingly increases by additional 170% to 4.32 mA cm^{-2}, which is the highest stable PEC water oxidation current for hematite photoanode ever reported.[6]

The Co–Pi can be prepared by several methods such as electrodeposition,[10] photodeposition,[4,18] photo-assisted electrodeposition,[6] and two-step chemical immersion.[28] Among them, Choi and co-workers[4,18] reported a facile method to form Co–Pi on the surface of some n-type semiconductors such as ZnO and α-Fe_2O_3 by photochemical deposition (photodeposition). The distinctive advantage of the photodeposition for coupling Co–Pi with a photoanode is that the photodeposition method has the effect of placing Co–Pi on the most active sites on the semiconductor surface for solar O_2 evolution. This self-site-selective photodeposition of Co–Pi can make the most effective use of Co–Pi and enhance O_2 evolution with a minimal amount of Co–Pi.[4]

In our previous work,[29,30] we have reported that dendritic α-Fe_2O_3 nanowire array films with high surface area can be formed *via* thermal oxidation of the electrodeposited dendritic α-Fe nanowires. The photocurrent density of the dendritic α-Fe_2O_3 nanowires was lower than the other reported nanowires and nanotubes, which may be attributed to higher e^-–h^+ recombination probability or the presence of higher amount of surface defects.[9,30] Herein, for enhancing the photocatalytic activities, the Co–Pi was coupled to the α-Fe_2O_3 films with different structures by the facile photodeposition method.

2. Experimental

The electrodeposition of α-Fe films were carried out in a conventional three-electrode cell system using a PysioLab potentiostat (Model KST-P1) as the similar process as our previous report.[29,30] The commercial indium-doped tin oxide (ITO: 50 mm × 5 mm) (ITO film thickness 200 nm, resistance ≤ 10 Ω cm^{-2}) coated glass substrate was used as working electrode. ITO glass substrate was dipped into the electrolyte solution vertically and the deposition area was fixed to 0.5 cm^2 (10 mm × 5 mm) by a Scotch tape. A coiled platinum wire and Ag/AgCl (in 3.0 M NaCl) electrode were used as counter and reference electrodes, respectively. All potentials in this work were measured *versus* Ag/AgCl electrode. All the electrodeposition experiments were carried out at room temperature (~24 °C) without stirring or any external gas bubbling. α-Fe films were deposited in 5 mL aqueous solution containing 0.05 M $FeSO_4$ and 0.1 M Na_2SO_4 aqueous solution with pH 2.5 (adjusted by adding 5.0 M and 1.0 M H_2SO_4) at +1.5 V for given time. α-Fe_2O_3 films were obtained by calcination of α-Fe films in air at 500 °C for 3 h (heating speed 2 °C min^{-1}) in furnace. Photodeposition of Co–Pi on the α-Fe_2O_3 films was carried out all at once in a glass Petri dish (9 cm in diameter) containing 40 mL solution of 0.5 mM $CoCl_2$ and 0.1 M potassium phosphate buffer at pH 7 under a hand-held UV lamp (Spectroline, Model ENF-260C/FE, λ = 365 nm) with an irradiance of 0.15 mW cm^{-2} measured by a Lutron UV light meter (Model YK-34UV) at room temperature (~24 °C) for 3 h.

X-ray diffraction (XRD, Rigaku miniFlex-II desktop, Cu Kα) patterns, transmission electron microscope (TEM, JEOL, JEM-2100F) with energy-dispersive spectroscopy (EDS, Oxford Instruments, INCA X-sight), scanning electron microscope (SEM, Hitachi S-4300) were used to check crystallinity, crystal structure, elemental composition, and surface and cross-sectional morphologies of the obtained films. Photoelectrochemical measurements were conducted with a potentiostat/galvanostat (Compactstat, Invium technologies) in a V-style three-electrode electrochemical cell equipped with quartz window at room temperature under 1 sun (Asahi HAL-320 solar simulator) illumination, employing a Pt foil and an Ag/AgCl (in 3.0 M NaCl) electrode as counter and reference electrode, respectively. A 1.0 M NaOH aqueous solution (pH = 13.6) was used as electrolyte. Photocurrent–potential was measured using linear sweep voltammogram (LSV) method at a scan rate of 10 mV s^{-1} under continue 1 sun light. Photoresponse was checked using chronoamperometry method with chopped 1 sun light (light on and off: 20 s) at +0.22 V *vs.* Ag/AgCl. The stability of the films in PEC water splitting were carried out at +0.5 V *vs.* Ag/AgCl for around 2 h under 1 sun light. For checking the incident photon to electron conversion efficiency (IPCE) (HS Technologies, Korea), the absolute intensity of the monochromic incident light was measured by a standard silicon photodiode (model BS-500, Bunkoukeiki Co. Ltd., Japan). Electrochemical impedance spectroscopy (EIS) was checked using a potentiostat/galvanostat (Compactstat, Invium Technologies) in a frequency range of 0.05–10 kHz.[31]

3. Results and discussion

Fig. 1(a) shows the schematic drawing of experimental set-up with three electrode system, working electrode (WR: ITO glass), reference electrode (RE: Ag/AgCl in 3.0 M NaCl) and counter electrode (CE: coiled Pt wire). Herein, all the experiments were carried out with a pH value of 2.5 and applied potential of +1.5 V since they are appropriate parameters for 1-D dendritic iron wire array growth on the fixed-size ITO substrates as the discussion in our previous works.[29,30] As the further experimental processes and products are shown in Fig. 1(b–d), the as-deposited α-Fe films can be converted to α-Fe_2O_3 by calcination at 500 °C for 2 h in air; then a Co-based oxygen-evolution catalyst is covered on the surface of α-Fe_2O_3 films by photodeposition method.[4] The as-obtained α-Fe films are dark color and non-transparent when the given deposition times are more than 30 s. The transparent α-Fe film with grey color can be obtained at 10 s since there are very less deposits on the ITO substrate. After calcination, the color of these films was

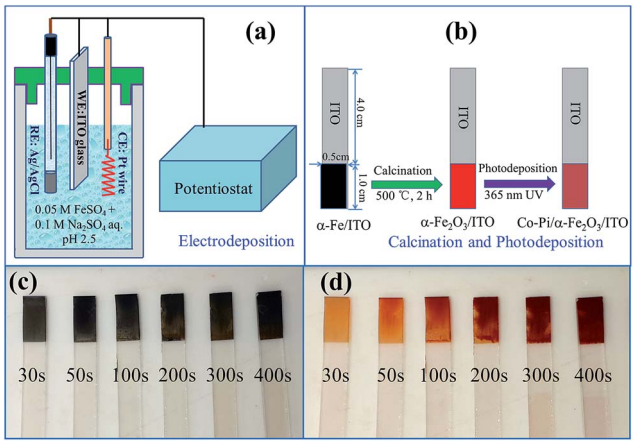

Fig. 1 Schematic diagrams showing (a) the experimental set-up and (b) the processes of formation of α-Fe_2O_3 and Co–Pi/α-Fe_2O_3 films from electrodeposited α-Fe films *via* calcination and photodeposition. (c) and (d) are the digital photographs of the electrodeposited α-Fe films at +1.5 V *vs.* Ag/AgCl for 30–400 s before and after calcination, respectively.

changed to yellow, red or dark red color, which depends on the film thickness. As the deposition time is increased, the transmittance is decreased and the films deposited longer than 300 s were non-transparent.

SEM images of α-Fe films are similar to the corresponding α-Fe_2O_3 films since the structures of the films are not changed by calcination.[29,30] Therefore, herein we only show the morphologies of α-Fe_2O_3 films, which were obtained by annealing the as-deposited α-Fe films, *via* SEM images as shown in Fig. 2(a–f). The α-Fe_2O_3 film, comes from the α-Fe film with the deposition time of χ seconds, is called α-Fe_2O_3-χ for short. The α-Fe_2O_3-30 film (Fig. 2(a)) is very compact and smooth; the similar morphology has been reported by Choi's group.[4] With 50 s deposition, the sparse dendrites with the length of *ca.* 3 μm are formed on the plate film. The α-Fe_2O_3-50 film (Fig. 2(b)) shows a plate film combined with the triangular hierarchical and dendritic structures. The dendrites of α-Fe_2O_3-100 films become longer wires, around 10 μm in length. The dendritic wires cannot stand vertically since they are soft and their densities are too low to give enough support to the neighbour dendritic wires.[32] In 200 s, 300 s and 400 s samples, the dendritic wires with the length of *ca.* 20, 35 and 50 μm, respectively, can stand vertically. In addition, some dendritic wires in some part of films lean slightly. This is caused by the washing process after electrodeposition. The α-Fe_2O_3-400 film has a similar surface construction with α-Fe_2O_3-300 film, but it contains higher dendrite density than the α-Fe_2O_3-300 film.

After photodeposition of Co–Pi for 3 h, there are no much difference in the color and the morphology change between the α-Fe_2O_3-χ film and the corresponding Co–Pi/α-Fe_2O_3-χ film. Therefore, we only show two typical Co–Pi/α-Fe_2O_3-χ films with $\chi = 30$ s (Fig. 3(a)) and 400 s (Fig. 3(b)) which represent the plate film and the dendritic array, respectively. It is easily observed that they are similar to the corresponding α-Fe_2O_3 films. It indicates that the photodeposited Co–Pi particles should be very small and cannot be distinguished by low-resolution SEM images. The detailed analysis is carried out by EDS elemental mapping, EDS spectrum and HRTEM as shown in Fig. 3(c–e). The similar Co and P element distribution mapping with Fe element indicates that the Co–Pi nanoparticles are uniformly deposited on the α-Fe_2O_3 dendrites surface. The ratio of Co to Fe is about 1.4 : 44.2. Co–Pi nanoparticles are easily distinguished

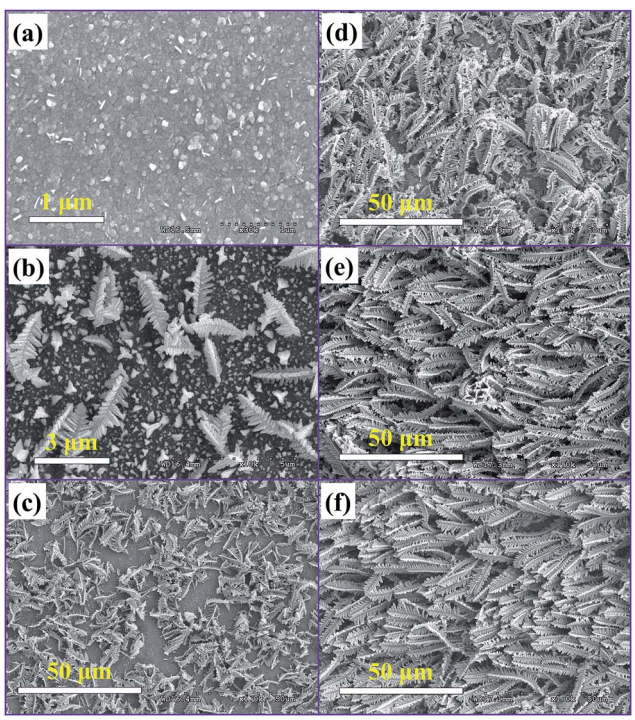

Fig. 2 (a–f) are the SEM images of α-Fe_2O_3 films obtained with different deposition times. (a) 30 s, (b) 50 s, (c) 100 s, (d) 200 s, (e) 300 s, and (f) 400 s.

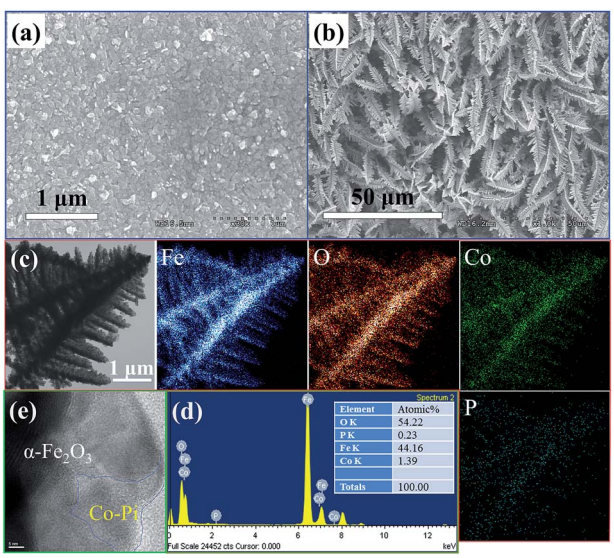

Fig. 3 (a) and (b) are the typical SEM images of Co–Pi/α-Fe_2O_3-χ films with $\chi = 30$ s and 400 s. (c) and (d) are the typical EDS elemental mapping and data. (e) is the HRTEM of Co–Pi/α-Fe_2O_3 structure.

from α-Fe_2O_3 grains by HRTEM images since Co–Pi is amorphous and α-Fe_2O_3 is crystalline as a typical image shown in Fig. 3(e). From the HRTEM image, it can be observed that the Co–Pi particles were deposited on the specific positions of the α-Fe_2O_3 surface, which gives an evidence for the self-site-selective photodeposition of Co–Pi.[4]

Fig. 4(a) shows XRD patterns of the typical (i) as-electrodeposited α-Fe, (ii) α-Fe_2O_3 and (iii) Co–Pi/α-Fe_2O_3 films. They can be perfectly indexed to α-Fe and α-Fe_2O_3 in terms of peak positions of JCPDS no. 65-4899 and 33-0664, respectively, as the same as our previous reports.[29,30] The baseline of the XRD pattern of Co–Pi/α-Fe_2O_3 film is hunched and has higher noise signals than pure α-Fe_2O_3 film, which is attributed to the amorphous Co–Pi nanoparticles. To assess the photocatalytic activity for solar water splitting, the photoelectrochemical properties containing of photocurrents and photoresponses for α-Fe_2O_3 and Co–Pi/α-Fe_2O_3 films were carried out in 1.0 M NaOH electrolyte solution (pH = 13.6) since the α-Fe_2O_3 photoanode is chemically stable in it.[33] The working electrodes (α-Fe_2O_3 or Co–Pi/α-Fe_2O_3 films) were immerged in the electrolyte and illuminated from the front side with 1 sun light by a solar simulator. The applied potentials were measured *versus* the Ag/AgCl reference electrode and can be converted to the reversible hydrogen electrode (RHE) scale using the following relationships.[31,34,35]

$$E_{RHE} = E_{Ag/AgCl} + E^0_{Ag/AgCl\ vs.\ NHE} + 0.0591 \times pH \quad (1)$$

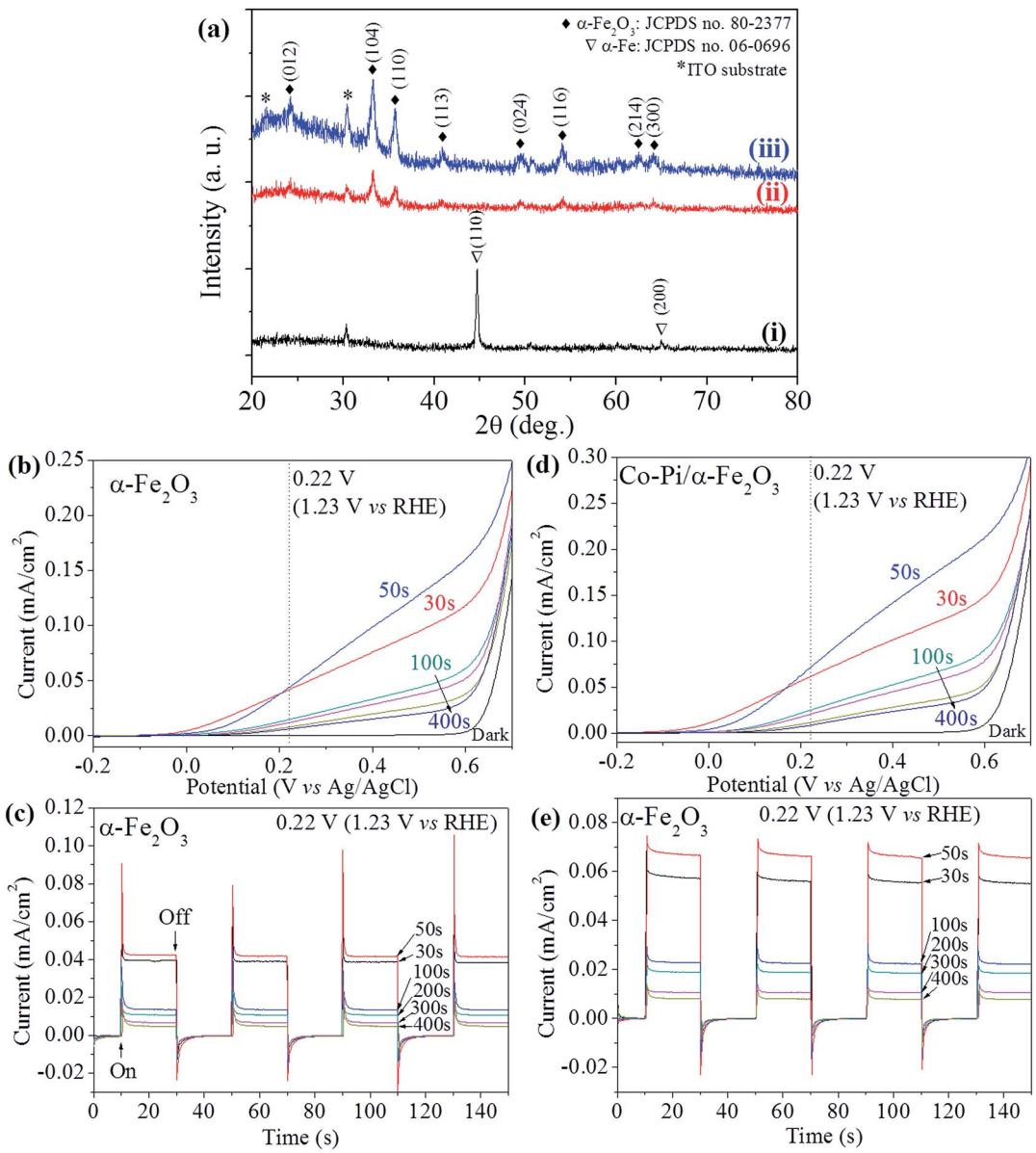

Fig. 4 (a) XRD patterns of the typical (i) electrodeposited α-Fe, (ii) α-Fe_2O_3 and (iii) Co–Pi/α-Fe_2O_3 films. Photocurrents and photoresponses of (b and c) α-Fe_2O_3-χ and (d and e) Co–Pi/α-Fe_2O_3-χ films in 1.0 M NaOH under continuing and chopped (on and off: 20 s) 1 sun light illumination. χ = 30, 50, 100, 200, 300 and 400 s.

with $E^0_{Ag/AgCl\ vs.\ NHE} = 0.209$ V at 25 °C and pH = 13.6:

$$E_{RHE} = E_{Ag/AgCl} + 0.209 + 0.0591 \times 13.6 \approx E_{Ag/AgCl} + 1.013\ V \quad (2)$$

where E_{RHE} is the converted potential *vs.* RHE, $E_{Ag/AgCl}$ is the experimental potential measured *versus* Ag/AgCl reference electrode. For example, the thermodynamic potential for water oxidation ($2H_2O \rightarrow O_2 + 4H^+ + 4e^-$, $E_{O_2/H_2O\ vs.\ NHE} = 1.23$ V at 25 °C) is ~0.22 V *vs.* Ag/AgCl at pH = 13.6, which is calculated by the eqn (2). The photocurrent and photoresponse curves of the α-Fe_2O_3 and Co–Pi/α-Fe_2O_3 films, prepared by the original electrodeposited α-Fe films *via* calcination and photodeposition, are shown in Fig. 4(b–e). As reported in the previous report,[10] the onset of a strong catalytic wave at 1.23 V *vs.* NHE was found in cyclic voltammetry of a 0.5 mM solution of $Co(NO_3)_2$ in 0.1 M potassium phosphate pH 7.0. In the linear sweep voltammetry process, the dark current of the Co–Pi/α-Fe_2O_3 films are zero at 1.23 V *vs.* NHE (0.22 V *vs.* Ag/AgCl), even at 1.5 V *vs.* NHE (0.5 V *vs.* Ag/AgCl). This is caused by several reasons. (i) The potential is dropped upon the resistances of the solution, the ITO substrate, and the α-Fe_2O_3; (ii) the amount of the Co–Pi on α-Fe_2O_3 is too less. It can be easily observed that the photocurrents of all α-Fe_2O_3 films are enhanced more or less after coupling with Co–Pi. The values of photocurrent densities at +0.22 V (1.23 V *vs.* RHE, the thermodynamic potential for electrolysis) and photocurrent onset potentials are shown in Table 1.

The photocurrent onset potentials of α-Fe_2O_3-χ films with $\chi = 30$, 50 and 100 s are the similar in the value of *ca.* −0.1 V; the others have the similar photocurrent onset potentials at 0 V. It can be easily observed that the α-Fe_2O_3-χ films with $\chi = 30$, 50 and 100 s can expose the bottom layer with large area and the bottom layers of $\chi = 200$, 300 and 400 s films are mostly covered with the dendritic structures. It indicates that the films with exposing thin bottom layer have relatively low photocurrent onset potentials and the films with relatively high density dendrites have high onset potentials. For a fine α-Fe_2O_3 particle film prepared by annealing the electrodeposited Fe film, the photocurrent onset potential can be as low as −0.4 V *vs.* Ag/AgCl as reported by Choi *et al.*[4] After coupling with Co–Pi *via* photodeposition, the photocurrent onset potential of Co–Pi/α-Fe_2O_3-χ with $\chi = 30$ and 50 s are shifted to negative direction by −0.1 and −0.05 V, respectively. The other films with $\chi = 100$ to 400 s are not shifted. It indicates that the Co–Pi/α-Fe_2O_3-χ with relatively short χ can give the more negative photocurrent onset potentials. The possible explanation is that in the photodeposition process the competition for deposition of Co–Pi between the bottom layer and upper dendritic structures was existed; under considerations of the light intensity decay and the reduced concentration gradient, the Co–Pi should be primarily deposited on the dendritic structures rather than on the bottom layer. The photocurrent of a stable photoelectrode (photoanode or photocathode) in PEC system is determined by the difference between the current with and without light illumination. Herein, we show the photocurrent values at +0.22 V for comparison since the value of +0.22 V is the thermodynamic potential for water oxidation in our PEC system as mentioned above. The photocurrents of Co–Pi/α-Fe_2O_3-χ films with $\chi = 30$ to 400 s are 57.2, 66.8, 22.8, 18.9, 10.6 and 8.1 μA cm^{-2} at +0.22 V, which are increased by 43%, 57.5%, 67.6%, 75%, 58.2% and 68.8%, respectively, compared with their initial α-Fe_2O_3 films. Obviously, the photocurrents of the bare α-Fe_2O_3 and Co–Pi/α-Fe_2O_3, especially the dendritic films with thicker thickness, are very low. Several possible attenuation factors should be mentioned in these dendritic films: the higher e^-–h^+ recombination probability or the presence of higher amount of surface defects.[9,30] In addition, as shown in Fig. 5(a) and (b), the length of dendritic α-Fe_2O_3 wires, obtained at long time deposition, is too long for electrons transferring from the top to the bottom because the long electron pathway could enhance the probability of e^-–h^+ recombination. In addition to it, the longer dendritic α-Fe_2O_3 wires films have much higher charge-transfer resistance (R_{ct}), which were investigated by the electrochemical impedance spectra (EIS) as shown in Fig. 5(c). Under the dark, the R_{ct} of three samples tends to infinity, which indicates that the huge charge-transfer resistance exists at the interface between the electrode and the electrolyte even with an external potential of +0.22 V.[31] Under 1 sun light illumination, all the R_{ct} of three samples are reduced. The photogenerated charge carriers (e^-–h^+) can be separated for the water splitting reactions. Especially, the R_{ct} of α-Fe_2O_3-χ films with $\chi = 30$ and 50 s

Table 1 The values of photocurrent onset potentials and photocurrent densities at +0.22 V (1.23 V *vs.* RHE) for different samples, α-Fe_2O_3-χ and Co–Pi/α-Fe_2O_3-χ with $\chi = 30$, 50, 100, 200, 300 and 400 s. ΔI is the difference between the photocurrent of α-Fe_2O_3 ($I_{\alpha\text{-}Fe_2O_3}$) and its corresponding photocurrent of Co–Pi/α-Fe_2O_3 ($I_{Co-Pi/\alpha\text{-}Fe_2O_3}$), $\Delta I = I_{Co-Pi/\alpha\text{-}Fe_2O_3} - I_{\alpha-Fe_2O_3}$. δ is the enhanced percentage of the photocurrent after coupling with Co–Pi, $\delta = \dfrac{\Delta I}{I_{\alpha\text{-}Fe_2O_3}} \times 100\%$

Samples	Photocurrent onset potential (V)			Photocurrent at +0.22 V (μA cm^{-2})		
χ	α-Fe_2O_3	Co–Pi/α-Fe_2O_3	ΔE_{onset}	α-Fe_2O_3	Co–Pi/α-Fe_2O_3	$\Delta I(\delta)$
30 s	−0.1	−0.2	−0.1	40.0	57.2	17.2 (43%)
50 s	−0.1	−0.15	−0.05	42.4	66.8	24.4 (57.5%)
100 s	−0.1	−0.1	0	13.6	22.8	9.2 (67.6%)
200 s	0	0	0	10.8	18.9	8.1 (75%)
300 s	0	0	0	6.7	10.6	3.9 (58.2%)
400 s	0	0	0	4.8	8.1	3.3 (68.8%)

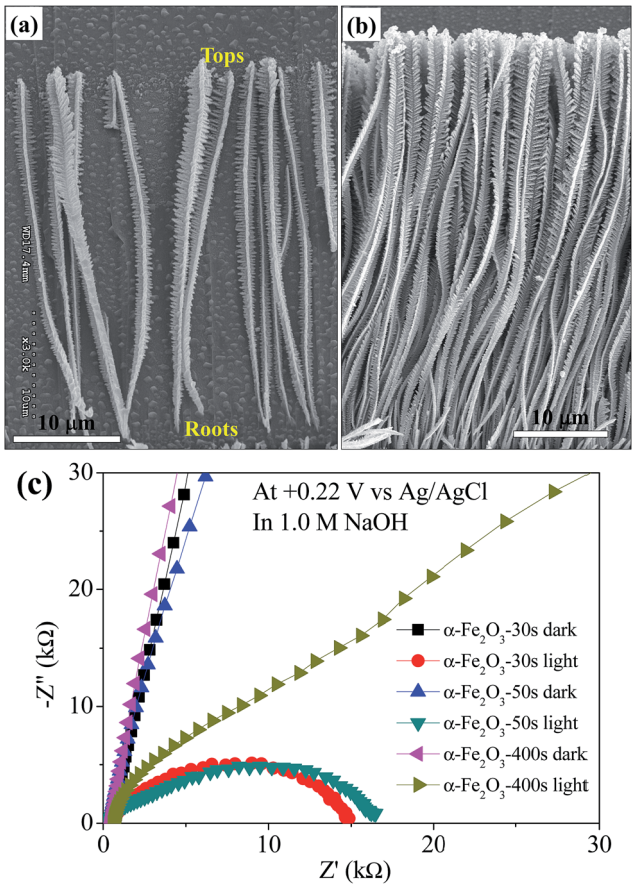

Fig. 5 (a) and (b) SEM images of the separated α-Fe_2O_3 dendritic wires and the α-Fe_2O_3 dendritic wire array obtained at the electrodeposition time of 300 s. (c) EIS of α-Fe_2O_3-χ films with χ = 30, 50, and 400 with and without light illumination, which were conducted in 1.0 M NaOH solution at +0.22 V *vs.* Ag/AgCl.

are decreased more. Therefore, the photocurrents of the α-Fe_2O_3 wires films obtained at short time (30 and 50 s) deposition are much better than long time deposition (>100 s). Recently, Shen[36] also mentioned that only low photocurrents were obtained because the dendritic hematite wires obtained at the long time deposition were too long to achieve effective light absorption and extract the photogenerated electrons to the substrate. To get the better photoelectrochemical performance of hematite films, the ideal nanostructure is a nanowires array with diameter of 5–10 nm and length of 400–500 nm.[9] After coupling with the Co–Pi co-catalyst, it is surprised that the photocurrent densities of most films can be enhanced by more than 50% regardless of the low photocurrent values at +0.22 V. The large initial anodic spikes, which occurred in the photoresponse curves of α-Fe_2O_3 films when the light was irradiated suddenly, were extraordinarily decreased after coupling with Co–Pi as shown in Fig. 4(c) and (e). It indicates that the Co–Pi can highly suppress the electron–hole recombination. In addition, as the reported works,[4,24–26] the photodeposited Co–Pi on α-Fe_2O_3 surface can increase the total amount of photocurrent generated by suppressing e^-–h^+ recombination because of the formation of a Schottky-type heterojunction by working as co-catalyst and increases the photocurrent to O_2 conversion

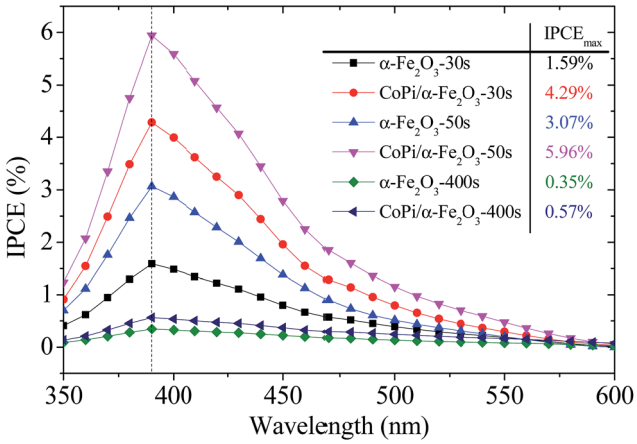

Fig. 6 IPCE for the typical α-Fe_2O_3-χ and Co–Pi/α-Fe_2O_3-χ films with χ = 30, 50, and 400 s. IPCEs were measured in 1.0 M NaOH solution at +0.5 V *vs.* Ag/AgCl.

efficiency by improving water oxidation kinetics; the Co–Pi and can also increase the lifetime of photogenerated holes in α-Fe_2O_3 photoanode.

The incident photon to electron conversion efficiencies (IPCEs) of the typical α-Fe_2O_3-χ and Co–Pi/α-Fe_2O_3-χ films with χ = 30, 50 and 400 s were carried out in 1.0 M NaOH at +0.5 V *vs.* Ag/AgCl under monochromic light illumination as shown in Fig. 6.

$$\mathrm{IPCE} = \frac{1240 \times j_p\ (\mathrm{mA\ cm^{-2}})}{P(\mathrm{mW\ cm^{-2}}) \times \lambda(\mathrm{nm})} \times 100\%$$

where j_p is the photocurrent density, P is the incident photon flux density at the photoelectrode location and λ is wavelength.[31] The maximum IPCE ($IPCE_{max}$) values of all films are achieved at the monochromic light of ~390 nm. The $IPCE_{max}$s of α-Fe_2O_3-χ and Co–Pi/α-Fe_2O_3-χ are 1.59% and 4.29% for χ = 30, 3.07% and 5.96% for χ = 50, and 0.35% and 0.57% for χ = 400, respectively. After coupling with Co–Pi, the $IPCE_{max}$s are increased by about 170%, 94%, and 63% for χ = 30, 50, and 400, respectively. The enhanced ratios are decreased as an increase

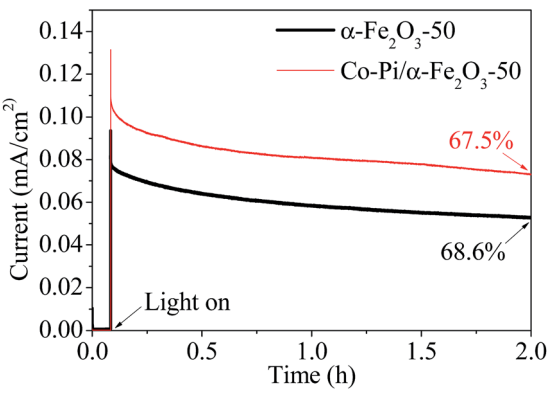

Fig. 7 Photocurrent–time curves of α-Fe_2O_3-50 and Co–Pi/α-Fe_2O_3-50 measured at +0.5 V *vs.* Ag/AgCl for ~2 h under 1 sun light illumination in 1.0 M NaOH solution.

in the density and length of dendrites. The stability of the optimized photoanodes of α-Fe_2O_3-50 and Co–Pi/α-Fe_2O_3-50 in PEC water splitting were determined by photocurrent–time curves as shown in Fig. 7, which were measured at +0.5 *vs.* RHE in 1.0 M NOH solution under 1 sun light illumination for ~2 h. The current curves in first 5 min were carried out in dark to show the stability and the current value without light illumination. The photocurrents of α-Fe_2O_3-50 and Co–Pi/α-Fe_2O_3-50 are 77.3 and 108.3 μA cm^{-2}, respectively, which are gradually decreased with an increase of the checking time. It indicates that both photoanodes are not so stable in PEC water splitting. However, the photocurrents of both electrodes can keep 68.6% and 67.5% of the initial photocurrent values after the PEC water splitting for ~2 h.

4. Conclusions

In summary, the α-Fe_2O_3 photoanodes with different structures can be easily prepared by calcination of the electrodeposited α-Fe films in air. The morphology of the film varies from nanoparticle to sparse dendrite, and then to close dendrite as the deposition time of α-Fe is prolonged. Their morphology-dependent photoelectrochemical properties are investigated through photocurrent and photoresponse. The α-Fe_2O_3 film exposing larger bottom particle layer area, such as α-Fe_2O_3-χ films with $\chi = 30$ and 50 s, has low photocurrent onset potential; after coupling with Co–Pi co-catalyst, their onset potentials are shifted to negative direction. The α-Fe_2O_3-50, be composed of the bottom particle layer and the loose dendrites with short length, has the best photoelectrochemical performance with the photocurrent density of 66.8 μA cm^{-2} at +0.22 V *vs.* Ag/AgCl. The photocurrent of hematite films can be enhanced by more than 40%; especially, high-density dendrite films can be increased by around 70% regardless of low photocurrent values. It indicates that photodeposited Co–Pi can effectively suppress the photogenerated electron–hole recombination. This work provides a useful insight for the comparison of the different structuring hematite films and gives a direction to preparing the hematite films with high photoelectrochemical performance for water splitting. The work for decreasing the charge transfer resistance is undergoing to enhance the photocurrent of dendritic film.

Acknowledgements

This work financially supported by the Korea Center for Artificial Photosynthesis (KCAP) located in Sogang University (no. 2009-0093885) funded by the Minister of Science, ICT and Future Planning (MSIP) through the National Research Foundation of Korea and the Brain Korea 21 Plus Project 2014.

Notes and references

1 A. Fujishima and K. Honda, *Nature*, 1972, **238**, 37.
2 K. Hashimoto, H. Irie and A. Fujishima, *Jpn. J. Appl. Phys., Part 1*, 2005, **44**, 8269.
3 D. K. Zhong, J. Sun, H. Inumaru and D. R. Gamelin, *J. Am. Chem. Soc.*, 2009, **131**, 6086.
4 K. J. McDonald and K.-S. Choi, *Chem. Mater.*, 2011, **23**, 1686.
5 J. S. Jang, K. Y. Yoon, X. Xiao, F.-R. F. Fan and A. J. Bard, *Chem. Mater.*, 2009, **21**, 4803.
6 J. Y. Kim, G. Magesh, D. H. Youn, J.-W. Jang, J. Kubota, K. Domen and J. S. Lee, *Sci. Rep.*, 2013, **3**, 2681.
7 J. H. Kennedy and K. W. Frese Jr, *J. Electrochem. Soc.*, 1978, **125**, 709.
8 U. Björkstén, J. Moser and M. Grätzel, *Chem. Mater.*, 1994, **6**, 858.
9 P. S. Bassi, Gurudayal, L. H. Wong and J. Barber, *Phys. Chem. Chem. Phys.*, 2014, **16**, 11834.
10 M. W. Kanan and D. G. Nocera, *Science*, 2008, **321**, 1072.
11 M. W. Kanan, Y. Surendranath and D. G. Nocera, *Chem. Soc. Rev.*, 2009, **38**, 109.
12 X. B. Han, Z. M. Zhang, T. Zhang, Y. G. Li, W. Lin, W. You, Z. M. Su and E. B. Wang, *J. Am. Chem. Soc.*, 2014, **136**, 5359.
13 M. D. Symes, Y. Surendranath, D. A. Lutterman and D. G. Nocera, *J. Am. Chem. Soc.*, 2011, **133**, 5174.
14 S. Y. Reece, J. A. Hamel, K. Sung, T. D. Jarvi, A. J. Esswein, J. J. H. Pijpers and D. G. Nocera, *Science*, 2011, **334**, 645.
15 Y. Qu and X. Duan, *Chem. Soc. Rev.*, 2013, **42**, 2568.
16 M. D. Kärkäs, O. Verho, E. V. Johnston and B. Åkermark, *Chem. Rev.*, 2014, **114**, 11863.
17 X. Li, J. Yu, J. Low, Y. Fang, J. Xiao and X. Chen, *J. Mater. Chem. A*, 2015, **3**, 2485.
18 E. M. P. Steinmiller and K. S. Choi, *Proc. Natl. Acad. Sci. U. S. A.*, 2009, **106**, 20633.
19 S. K. Pilli, T. E. Furtak, L. D. Brown, T. G. Deutsch, J. A. Turner and A. M. Herring, *Energy Environ. Sci.*, 2011, **4**, 5028.
20 T. H. Jeon, W. Choi and H. Park, *Phys. Chem. Chem. Phys.*, 2011, **13**, 21392.
21 D. E. Wang, R. G. Li, J. Zhu, J. Y. Shi, J. F. Han, X. Zong and C. Li, *J. Phys. Chem. C*, 2012, **116**, 5082.
22 F. F. Abdi, N. Firet and R. van de Krol, *ChemCatChem*, 2013, **5**, 490.
23 E. R. Young, R. Costi, S. Paydavosi, D. G. Nocera and V. Bulovic, *Energy Environ. Sci.*, 2011, **4**, 2058.
24 M. Barroso, A. J. Cowan, S. R. Pendlebury, M. Grätzel, D. R. Klug and J. R. Durrant, *J. Am. Chem. Soc.*, 2011, **133**, 14868.
25 D. K. Zhong, M. Cornuz, K. Sivula, M. Grätzel and D. R. Gamelin, *Energy Environ. Sci.*, 2011, **4**, 1759.
26 Q. Zeng, J. Bai, J. Li, L. Xia, K. Huang, X. Li and B. Zhou, *J. Mater. Chem. A*, 2015, **3**, 4345.
27 J. Yang, D. Wang, H. Han and C. Li, *Acc. Chem. Res.*, 2013, **46**, 1900.
28 L. Fu, H. Yu, C. Zhang, Z. Shao and B. Yi, *Electrochim. Acta*, 2014, **136**, 363.
29 R. Qiu, J. Y. Zheng, H. G. Cha, M. H. Jung, K. J. Lee and Y. S. Kang, *Nanoscale*, 2012, **4**, 1565.
30 J. Y. Zheng, M. J. Kang, G. Song, S. I. Son, S. P. Suh, C. W. Kim and Y. S. Kang, *CrystEngComm*, 2012, **14**, 6957.
31 J. Y. Zheng, G. Song, J. Hong, T. K. Van, A. U. Pawar, D. Y. Kim, C. W. Kim, Z. Haider and Y. S. Kang, *Cryst. Growth Des.*, 2014, **14**, 6057.

32 J. Y. Zheng, Z. L. Quan, G. Song, C. W. Kim, H. G. Cha, T. W. Kim, W. Shin, K. J. Lee, M. H. Jung and Y. S. Kang, *J. Mater. Chem.*, 2012, **22**, 12296.
33 P. S. Shinde, G. H. Go and W. J. Lee, *J. Mater. Chem.*, 2012, **22**, 10469.
34 X. Zhang, Y. Liu, S. T. Lee, S. Yang and Z. Kang, *Energy Environ. Sci.*, 2014, **7**, 1409.
35 G. Read, Y. Park and K.-S. Choi, *J. Phys. Chem. Lett.*, 2012, **3**, 1872.
36 S. Shen, *J. Mater. Res.*, 2014, **29**, 29.